Temperature-dependent magnetization in bimagnetic nanoparticles with antiferromagnetic interfacial exchange

N. R. Anderson and R. E. Camley
UCCS BioFrontiers Center, 1420 Austin Bluffs Parkway, Colorado Springs, Colorado 80918, USA
(Received 25 April 2016; revised manuscript received 1 September 2016; published 31 October 2016)

We present a self-consistent local mean-field analysis of core-shell nanoparticles with ferromagnetic materials but with antiferromagnetic interface exchange coupling. The importance of this type of structure for a variety of applications, including biomedical applications and magnetic recording, has been emphasized in recent studies of core-shell nanoparticles of iron and manganese oxides. We develop theoretical results for a different combination of materials that also have antiferromagnetic coupling, namely nanoparticles composed of Fe and Gd, and show how the magnetic properties depend on temperature and applied field. We examine results for the case where Gd is the core material and Fe is the shell and vice versa, as well as the results for an Fe/Gd alloy. We find that the size of the core (typically 4–5 nm in diameter) and shell (typically < 2 nm wide) and the combined size of the nanoparticle all affect the magnetic behavior of the system. As the temperature is varied, the particles go through multiple phases, including one where the core magnetic moment is aligned with an external field, one where the shell magnetic moment is aligned with an external field, and one where the core and shell magnetic moments are in a canted state (occurring for fields larger than 2 kOe). In addition, we calculate the net magnetic moment versus temperature for the various structures and show that the compensation temperature (where the net magnetic moments of the Fe and Gd nearly cancel) depends on all the material parameters—the core radius, the shell radius, and the magnetic field. We also examine the thermal stability of these structures and show that the nanoparticles can effectively be ferromagnetic at both low and high temperatures and show superparamagnetic-like behavior in the 200–300 K range.

DOI: 10.1103/PhysRevB.94.134432

I. INTRODUCTION

Magnetic nanoparticles and heterostructures have received significant attention [1–5] due to the need for various material properties not found in homogeneous materials. Already a number of these heterostructures are seen in electronic devices, hard drives, MRI contrast agents, and a number of biomedical applications [6–8]. Bimagnetic nanoparticles have so far been shown to allow for flexibility in remnant magnetization, coercive field, compensation temperature [9], exchange bias [10] and net magnetization [11]. Bimagnetic nanoparticles, typically where one magnetic material comprises the homogeneous core and a second magnetic material acts as a spherical shell, may allow for large-scale production without the limitations of thin films.

A number of bimagnetic nanoparticles have already been fabricated. However, until recently all bimagnetic nanoparticles were restricted to ferromagnetic (FM) coupling between the core and shell materials or coupling between a ferromagnet and antiferromagnet. Novel behavior between the core and shell coupling directions has been found for various structures including a homogeneous sphere [12] and hard-soft core-shell nanoparticles [13] and layered structures [14]. The antiferromagnetic (AFM) interface coupled nanoparticles have been produced both with a hard magnetic material as the core and a soft magnetic material as the shell and also vice versa. These two types of nanoparticles show a variety of different behaviors from one another.

Similar structures have been analyzed theoretically before [15–17] including layered structures with AFM interface coupling [18] and cubic structures using an Ising model [19]. However, the change to a spherical geometry changes the number and type of boundaries for cells, especially at the surface of the structure. The addition of these boundaries has a large effect on the transition of the magnetization with temperature. The use of an Ising model requires spins to be parallel or antiparallel with the external field, meaning a canted state between spins is neglected. Another recent study has used a fast Monte Carlo method to look at dipole interactions between nanoparticles with AFM interactions [20].

The use of materials that have AFM interfacial coupling could lead to new effects or enhancements of desired effects in nanoparticles. This type of structure allows multiple transitions between states as temperature changes and in turn has novel magnetization characteristics. The bimagnetic structure allows for a compensation temperature, a temperature where the net magnetic moment is zero due to the antialignment of the core and shell, and the different temperature dependencies of the constituent materials. We find that the compensation temperature can be altered from 0 to above 300 K by changing the radius of the core in a bimagnetic core-shell nanoparticle. In addition, the slope of the magnetization vs temperature can be made to increase, decrease, or remain approximately constant over more than 400 K by appropriately selecting the size and material for the core and shell. We also find that these core-shell particles can be made to have larger or smaller thermal stabilities at a variety of temperatures.

In this paper we use a self-consistent local mean-field theory to analyze the behavior of two AFM-coupled FM materials. As an example we choose Fe and Gd because these materials have been well characterized in layered structures, and have very different Curie temperatures, leading to interesting thermal behavior for the nanoparticle. As has been recently emphasized [21], the self-consistent mean-field approach is an efficient way to gain physical insight into

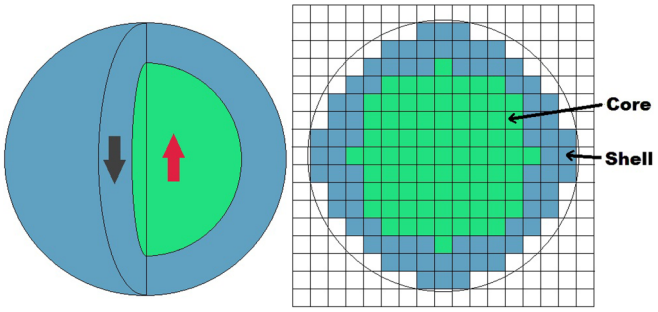

FIG. 1. A sample geometry and the associated discretization of the core-shell nanoparticle.

complex problems. We analyze the thermal-averaged magnetic moment on each atom as well as the total thermally dependent magnetic moment for the structure. The results provide a range of interesting behavior which can be controlled by particle size, applied field, temperature, and shell thickness.

II. THEORY

A sample geometry for the calculations is shown in Fig. 1. Each cell contains a single Fe atom, a single Gd atom, or is empty. The cell structure is simple cubic. The total spin in each cell is either $S = 3.5$ for Gd or $S = 1$ for Fe.

The equilibrium structure is calculated in the following way. First, one assigns values for the spin magnitude and orientation in each cell. Then one picks a cell n at random and finds the effective magnetic field acting on that cell,

$$\vec{H}(n) = \vec{H}_{ex}(n) + H_0\hat{z}. \tag{1}$$

This field is composed of the exchange field and the external field. We have neglected anisotropy and dipolar fields because these are typically much smaller than the exchange field. For example the magnetocrystalline anisotropy field for Fe is roughly 300 Oe and Gd is 100 Oe. Similarly the dipole field for the Gd atom at a neighboring site is the exchange field and is found by summing over nearest-neighbor cells:

$$\vec{H}_{ex}(n) = \frac{1}{g\mu_B}\sum_{m=nn} J_{nm}\langle\vec{S}(m)\rangle, \tag{2}$$

where $\langle\vec{S}(m)\rangle$ is the thermal-averaged spin at the nearest-neighbor site m. The values of the effective exchange constants may be estimated from the Curie temperatures of the two materials and are given by the formula [22]

$$J = \frac{3k_BT_C}{zS(S+1)}, \tag{3}$$

where T_C is the Curie temperature, g is the Lande g factor, μ_B is the Bohr magneton, k_B is the Boltzmann constant, and z is the number of nearest neighbors; $z = 6$ in our model, which is appropriate for a simple cubic system. For Fe $T_C = 1043$ K and for Gd $T_C = 292$ K. This gives $J_{\mathrm{Fe}}/k_B = 260.75$ K and $J_{\mathrm{Gd}}/k_B = 9.3$ K. There is an antiferromagnetic interface exchange, as well, with a magnitude in between the two exchange constants above. We choose $J_i/k_B = -100.0$ K. Here both the Fe and interface exchange are large in magnitude compared to the Gd exchange, consistent with previous phenomenological models and experimental studies of the interaction between transition metals and rare-earth intermetallics [9,23]. We note that recent *ab initio* calculations validate our model in showing that the Fe-Gd exchange coupling is large and antiferromagnetic [24].

The magnetic moment in cell n is then aligned with the direction of the effective magnetic field acting on it, which lowers the energy of the system. In addition, the thermal-averaged magnitude of the spin at site n is found using the Brillouin function [22],

$$\langle S(n,T)\rangle = S(n)\left[\frac{2S(n)+1}{2S(n)}\coth\left(\frac{2S(n)+1}{2S(n)}X\right) - \frac{1}{2S(n)}\coth\left(\frac{X}{2S(n)}\right)\right] \tag{4}$$

and

$$X = g\mu_B\vec{S}(n)\cdot\vec{H}(n)/k_BT, \tag{5}$$

where T is the temperature.

Another site is chosen at random and the process is repeated until all spins are in a self-consistent state in terms of their orientation and thermal magnitude. The total magnetic moment of the nanoparticle, in the direction of the applied field, is found by

$$m_{\mathrm{tot}} = \sum_n g\mu_B\langle S_z(n)\rangle, \tag{6}$$

where S is the spin of Gd or Fe.

Multiple simulations with different starting orientations should be considered to ensure that an energy minimum for the system is found. The number of iterations per cell to find an equilibrium depends on the starting orientations as well as how near the system is to a phase transition. We have found that even near phase transitions 2×10^4 iterations per cell is typically sufficient for accurate results.

We note that this is a simplified model in terms of the spatial coordination and structure. Bulk Fe stacks in the bcc structure and bulk Gd in the hcp structure, but we treat both as simple cubic in this analysis. Of course a real nanoparticle with a spherical core-shell geometry may have voids, interdiffusion at the interfaces, and stacking defects and is unlikely to have the perfect bulk structure. This helps motivate our simple model, which will contain the key elements of the overall magnetic structure of the nanoparticle. The system is discretized with the side length of a cell of 0.228 nm, the nearest-neighbor distance for Fe.

The Brillouin function is appropriate for calculating the thermal-averaged moment of an individual spin in the local field produced primarily by exchange interactions. In this case a quantum mechanical calculation is appropriate. To calculate the alignment of the total magnetic moment for the structure with an external field the situation is different. Here thousands of atoms are considered and a classical calculation is appropriate. For this we use the Langevin function. In the limit when $S \to \infty$ the Brillouin function becomes the Langevin function, given by [25]

$$m(T)_{\mathrm{Langevin}} = m_{\mathrm{tot}}\left[\coth(X) - \frac{1}{X}\right]. \tag{7}$$

In this case,

$$X = \frac{m_{\text{tot}} H_0}{k_B T}, \tag{8}$$

the applied magnetic field is used instead of the applied field plus the exchange field. Also, m_{tot} is the sum of the thermal-averaged magnetic moment in each cell, found by using the Brillouin function. Using the Langevin function we can evaluate the total magnetic moment and determine for which sizes and shell thicknesses the ensemble becomes nonmagnetic. The Langevin function allows us to model the behavior of the nanoparticle as a function of temperature due to classical effects, resulting from changes to the structure as a whole rather than individual spins.

III. RESULTS

We analyze results for a variety of core-shell nanoparticles using Fe and Gd spherical layers. As noted earlier, these materials are both ferromagnetic, but at the interface between the two materials there is an AFM exchange coupling. Although the numerical outcomes for the magnetic configuration and $m_{\text{tot}}(T)$ are specific to these materials, the size of the particle, and the layering pattern, the general behavior of an AFM coupled system can be seen in our examples below. We also compare the results for $m_{\text{tot}}(T)$ between the core-shell structures and alloy structures with similar elemental compositions.

A. Core-shell configurations

There are three distinct magnetic configurations in the core-shell structure:

(1) Where Fe is aligned with the external field and Gd is either antiparallel to the external field or negligible in magnitude. This is referred to as the the Fe-aligned state.

(2) Where Gd is aligned with the external field and Fe is antiparallel. This is called the Gd-aligned state.

(3) A state where Fe and Gd are both partially aligned with the external field, called the canted state. In our geometry the external field is along the z axis, so in the canted state the Fe and Gd magnetic moments would both have components along the z axis but would also have components along another direction with opposite signs. For example Fe would have a $+x$ component and Gd would have a $-x$ component. The canted state is facilitated by the relatively small exchange field present in Gd. The AFM interface exchange forces the Gd atoms near the interface to align antiparallel to the external field, but there is a twist in the direction of the Gd moments as the distance from the interface is increased.

Typical configurations and a typical curve showing magnetic moment as a function of temperature are shown in Fig. 2. Here the particle has a Gd core with a radius of 21 cells and an Fe shell with a thickness of 10 cells and an applied field of 2 kOe. The three states are shown in Figs. 2(a)–2(c). The nonmonotonic behavior of the magnetic moment vs temperature (m vs T) curve in Fig. 2(d) is due to the transition from one state to another. For smaller applied fields there is a compensation point near "b". For larger applied fields the canted state dominates near "b" and persists through a large temperature range. For a large enough applied field, around 5 kOe, the nanoparticle is canted even at 0 K. For applied fields less than 2 kOe there is a transition from the Fe-aligned state to the Gd-aligned state, or vice versa, at the compensation temperature.

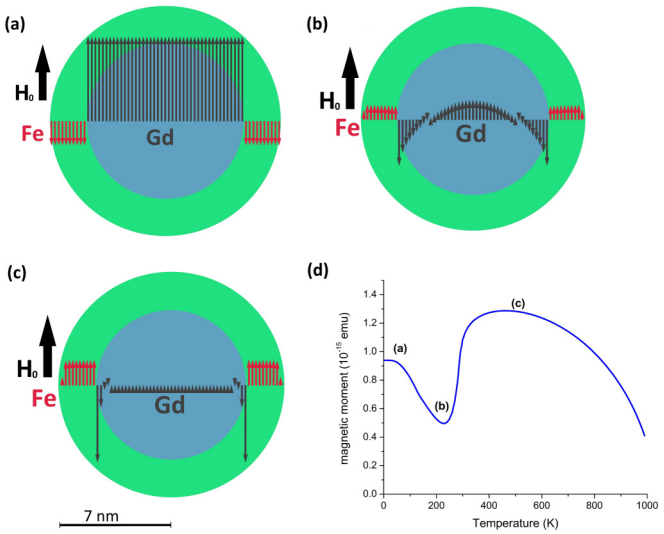

FIG. 2. In (a)–(c) are schematics showing the component of the thermal-averaged magnitude of the magnetic moment along a representative line of atoms through the center of the nanoparticle. In (a) we see the Gd-aligned state at 0 K, in (b) the canted state at 230 K, and in (c) the Fe-aligned state at 500 K where the Gd moments away from the interface go to zero magnitude. The radius of the particle is 31 atoms and the radius of the core is 21 atoms. (d) shows the magnetic moment vs temperature for the core-shell nanoparticle with a radius of 31 cells and a core radius of 21 cells. The applied field is 2 kOe, large enough to force the system into a canted state around 220 K. The locations of the states are marked with (a), (b), and (c) on the graph.

Surface effects are also evident in Figs. 2(b) and 2(c). Here the thermal-averaged magnitude of the magnetic moment of the outermost layer of Fe is decreased below 50% of the adjacent inner layers. This effect is more readily seen at higher temperatures. This can be explained by noticing that the value of X in Eq. (5) decreases as the effective field decreases, and, due to the self-consistent calculation, the effective fields on the outermost layer are small because of the reduced number of nearest neighbors. Similar effects are seen at lower temperatures when Gd is in the shell and Fe is in the core.

When the number of Fe cells is large the particle is in the Fe-aligned state at 0 K and remains in this state as T is increased. In contrast, if there are enough Gd cells the system is in the Gd-aligned state at 0 K and then transitions to Fe-aligned at higher temperatures. Figure 3 shows m vs T curves for a variety of core radii while the outer radius of the nanoparticle remains constant at 31 cells. In Fig. 3(a) all of the nanoparticles have an Fe core. Except for the core radius = 30 these particles have enough Gd to begin in the Gd-aligned state, and then transition to the Fe-aligned state above the compensation temperature. The particle with a core radius = 30 is in the Fe-aligned state at all temperatures, but shows an increase in magnetic moment as T is increased. However, in Fig. 3(b) the particles with

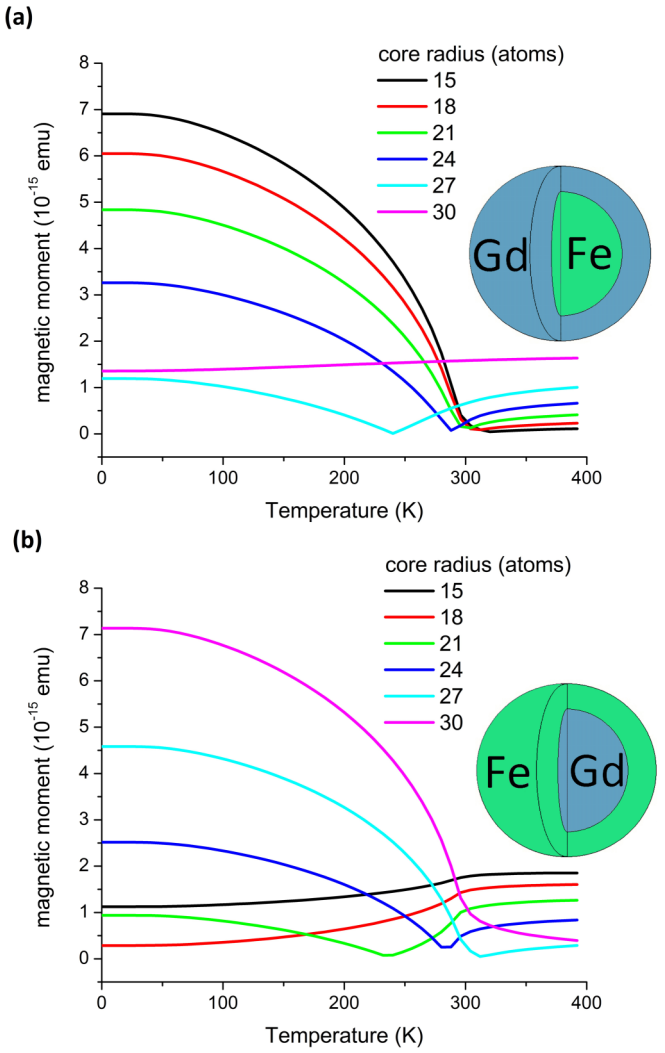

FIG. 3. A plot of m vs T for (a) Fe-core and Gd-shell nanoparticle and (b) Gd-core and Fe-shell nanoparticle. In both graphs the outer radius of the shell is kept constant at 31 atoms and the core radius is varied from 15 to 30 atoms. The applied field is $H_0 = 1$ kOe.

small core radii, core radius = 15 and 18, have enough Fe to maintain the Fe-aligned state for all temperatures. For all of the nanoparticles in the Gd-aligned state at 0 K the compensation temperature is closer to 0 K for particles containing less Gd. However, for nanoparticles in the Fe-aligned state at 0 K, the compensation temperature does not vary significantly but the magnitude of the 0 K magnetic moment increases for larger volume fractions of Fe. The compensation temperature can be tailored by adjusting the size of the core and changing the volume fractions of Fe and Gd. Likewise, at any given temperature the magnetic moment or the slope of m vs T can be tailored by a similar process.

Another interesting feature of these nanoparticles is that one can arrange to have a magnetic moment that increases, decreases, or remains nearly constant over a wide temperature range. For example, for an Fe core of radius 30 cells and Gd shell with thickness 1 cell [see Fig. 3(a)] at an applied field of 1 kOe the total moment of the particle increases with increasing temperature. This is because the Gd has a lower Curie temperature, so the thermal magnitude of the Gd moment decreases more quickly with increasing temperature compared to the Fe. In addition, the Gd is antialigned with the external field, so decreases in the magnitude of the Gd moment increase the total moment. However, as the temperature increases, the Fe, which is aligned with the external field, also decreases in magnitude. This has the effect of decreasing the total moment of the particle. These two effects can nearly cancel out leaving the particle with a constant magnetic moment through a temperature range determined by the volume fraction of the Fe and Gd. One can see a similar behavior in Fig. 3(b) as well for some compositions at temperatures above 300 K. However, a similarly sized nanoparticle of pure Fe shows a nearly constant magnetic moment between 0 and 400 K, decreasing by 0.08×10^{-15} emu at an applied field of 2 kOe.

Figure 4 shows an m vs T plot comparing alloyed particles with volume fractions of 33%, 45%, and 66% Gd to core-shell (Gd-Fe) nanoparticles with similar volume fractions of Gd and Fe. For the alloy, there are a larger number of Fe and Gd atoms interacting antiferromagnetically. Because J_i is large compared to J_{Gd} this leads to high-temperature stabilization of the Gd magnetic moment. This stabilization moves the compensation temperature higher for the alloy compared to the core-shell particle. However, for the core-shell nanoparticles the thermal stabilization of the Gd due to the AFM interaction primarily takes place at the interface between the core and shell. Due to this, the rest of the Gd moments rapidly decrease above the Gd Curie temperature and a magnetization due to the Fe is evident above the compensation temperature. Thus, the core-shell nanoparticles in some cases can have a larger thermal-averaged moment, compared to alloys, above

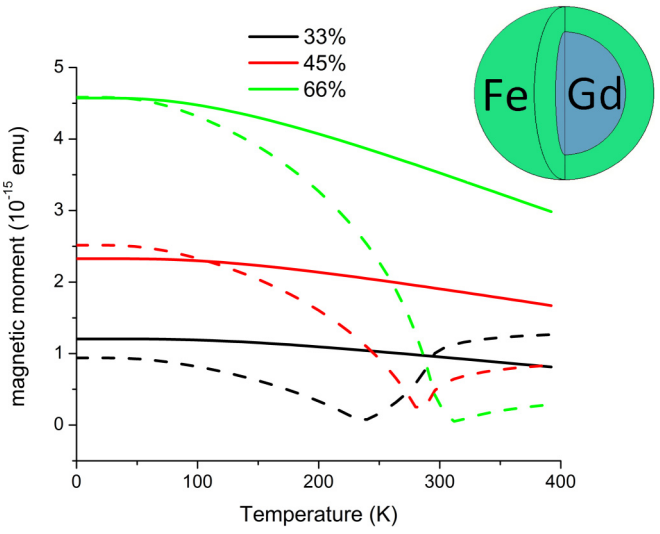

FIG. 4. An m vs T plot for a Gd-core and Fe-shell nanoparticle compared to an alloyed nanoparticle. The alloyed particle and core-shell nanoparticles have approximately the same volume fraction of Gd, 33%, 45%, and 66% for the black, red, and green curves, respectively. The solid lines are the alloyed particles and the dashed lines are the core-shell nanoparticles. The nanoparticles all have a radius of 31 atoms and the applied field is $H_0 = 1$ kOe.

the compensation temperature because there is no longer a significant cancellation from the antialigned Gd and Fe moments (see the 33% case in Fig. 4).

B. Superparamagnetic-like behavior

Superparamagnetism is the effect where the thermal energy becomes large enough to compete with the anisotropy energy for a given system. At this point fluctuations due to thermal energy cause a change in the orientation of the magnetic particle which occurs on a time scale shorter than the repetition time between measurements of the system. In this case the time-averaged measure of the magnetization decreases to 0. Our calculations have neglected anisotropy and instead consider the competition between Zeeman energy and thermal energy. While this is not a true measure of superparamagnetism for magnetic particles, it does give some information about the thermal stability of a structured nanoparticle. Below we use the term "superparamagnetic-like" behavior to determine the thermal stability for different core-shell configurations.

To explore the superparamagnetic-like behavior of core-shell nanoparticles we use the Langevin function, which accounts for thermal fluctuations acting on a global scale, rather than a local scale as the Brillouin function does. The total thermal-averaged moment found from the Brillouin function (solid curves) and the Langevin moment (dashed curves) are compared in Fig. 5(a) for an Fe-Gd core-shell particle of radius 31 atoms where the shell is 4 atoms thick. Similarly, in Fig. 5(b) a Gd-Fe core-shell particle is shown. In both Figs. 5(a) and 5(b)

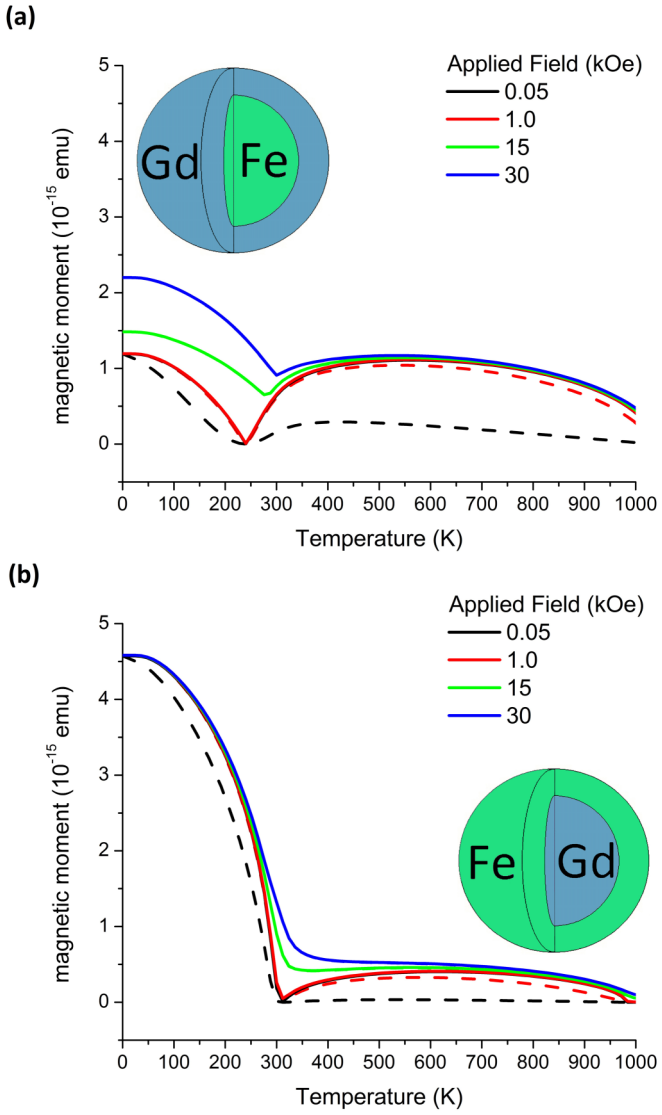

FIG. 5. In (a) an m vs T plot for an Fe-core and Gd-shell nanoparticle is shown. In (b) an m vs T plot for a Gd-core and Fe-shell nanoparticle is shown. Both graphs show the Langevin moment, as dashed curves, and the total thermal-averaged moment, as solid curves, for a variety of applied fields. All particles have a radius of 31 atoms and a core radius of 27 atoms.

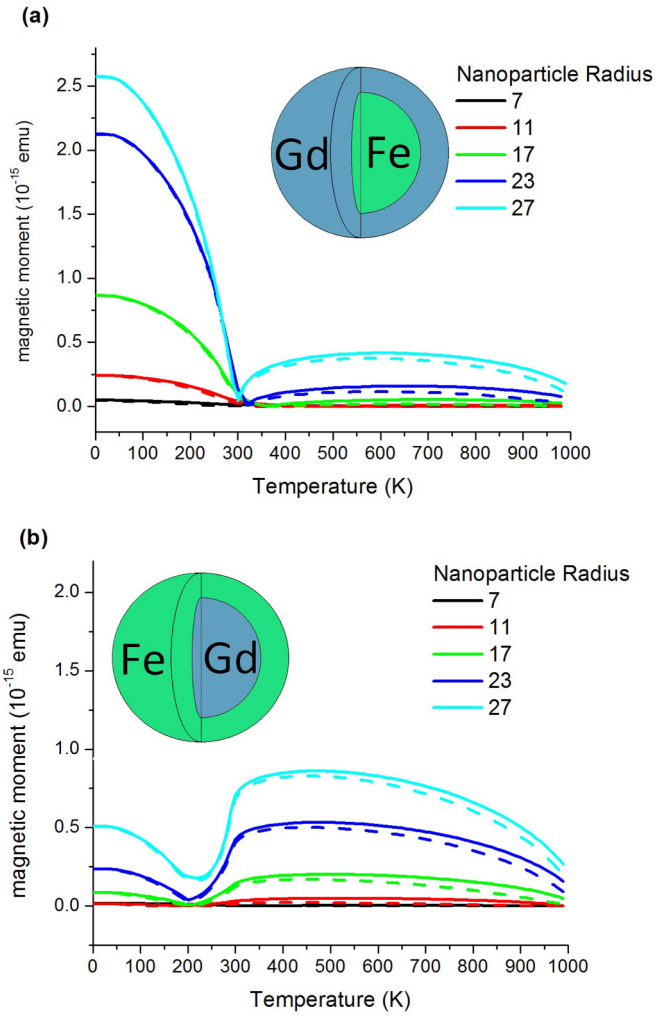

FIG. 6. In (a) an m vs T plot for an Fe-core and Gd-shell nanoparticle is shown. In (b) an m vs T plot for a Gd-core and Fe-shell nanoparticle is shown. Both graphs show the Langevin moment, as dashed curves, and the total thermal-averaged moment, as solid curves, for a variety of radii of nanoparticles. All particles have a similar ratio of core to total volume, approximately 40%. The applied field is 2 kOe. At this field a canted state is evident in (b) for the radius = 27 atom curve.

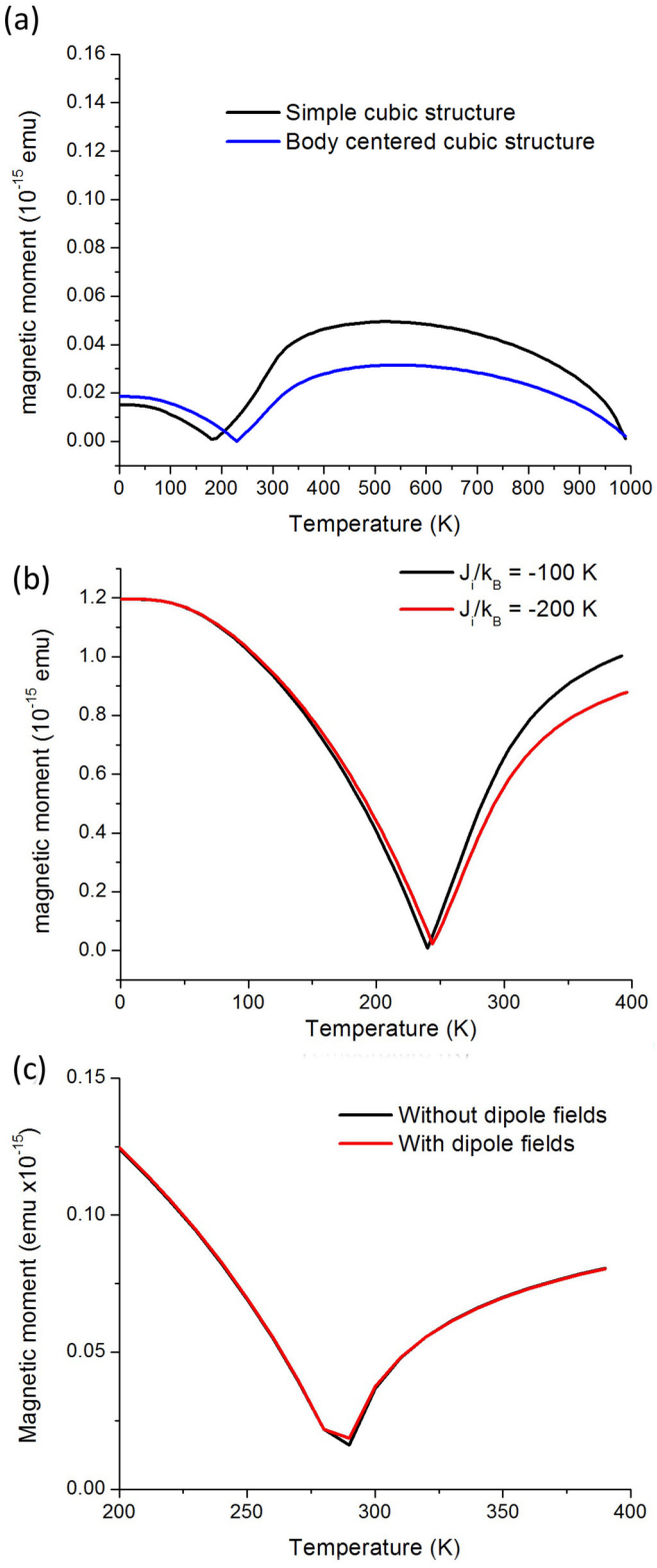

FIG. 7. In (a) a comparison for calculations done using a simple cubic lattice (black) and a body-centered cubic lattice (blue) where the structure is a Gd core of radius 7 atoms and an Fe shell with thickness 4 atoms in a 2 kOe applied field. In (b) a comparison of two identical spherical core-shell structures except where the interface exchange parameter has been changed from $J_i/k_B = -100$ K (black) to $J_i/k_B = -200$ K (red). Here the Fe core has a radius of 27 atoms, the Gd shell has a thickness of 4 atoms, and there is a 2 kOe applied field. In (c) a comparison between a calculation with only exchange interactions and a Zeeman interaction (black) and a calculation with exchange, Zeeman, and dipole-dipole interactions between all atoms (red). The Gd core has a radius of 11 atoms and an Fe shell thickness of 4 atoms in a 5 kOe applied field.

the curves for applied fields ranging from 50 Oe to 30 kOe are shown.

For both core-shell particles there is a significant low-temperature magnetic moment even for small applied fields. The superparamagnetic-like effect becomes easily noticeable for applied fields less than $H_0 = 1$ kOe. Especially for the $H_0 = 0.05$ kOe applied field case shown in in Fig. 5(a), we notice decreased thermal stability in the 200–300 K range where the Fe and Gd moments nearly cancel. For larger applied fields we see large magnetic moments for these particles which are approximately 15 nm in diameter. In the case of the Fe-Gd nanoparticle there is still a noticeable Langevin moment above the compensation temperature for $H_0 = 50$ Oe while for the Gd-Fe nanoparticle there is not.

Decreasing the size of the nanoparticles tends to make them thermally unstable with respect to alignment with the external field and move them into the superparamagnetic regime. We explore whether this is an important issue for smaller nanoparticles in Fig. 6. In Figs. 6(a) and 6(b) we compare the magnetic moments of Fe-Gd and Gd-Fe core-shell nanoparticles, respectively. The external applied field is 2 kOe and the core is approximately 40% of the total volume for all sizes of nanoparticles. In both figures we see that the Langevin moment does not vary considerably from the thermal-averaged moment except above 400 K. At an applied field of 2 kOe we see the presence of the canted state in Fig. 6(b) for nanoparticle radii larger that 23. This is apparent because the total thermal-averaged magnetic moment does not go to zero in the transition from the Gd-aligned state to the Fe-aligned state. However, for smaller sizes the Gd core is too small and the Gd exchange field, compared to the applied field, is too large to allow a canted state. The magnetic moment is seen to rapidly diminish as the size is decreased due to the antialignment of the core and shell along with the increased ratio of surface spins to volume spins. For the sizes considered here, we see that the particles tend to be thermally stable, without a large difference between the Brillouin and Langevin moments. However real structures are likely to have voids and other imperfections leading to a reduced magnetization and thermal stability and superparamagnetism is likely to be an issue for those structures.

We now discuss the validity of some of our assumptions.

(1) We have assumed a simple cubic lattice for both the Fe and Gd. We can test this assumption by comparing results from a calculation done with a simple cubic (sc) lattice to those using a body-centered cubic (bcc) lattice. We find qualitatively similar results using both lattice types for a variety of different sizes of nanoparticles. An example of this is shown in Fig. 7(a) for a structure with a Gd core (radius 7 atoms) and an Fe shell (thickness 4 atoms) with an applied field of $H_0 = 2$ kOe. The ratio of Gd atoms to Fe atoms is 34.8% for the bcc structure and 34.1% for the sc structure. Qualitatively all the behaviors seen

in the results for the simple cubic structure are also found in the bcc structure. The disparity in the quantitative results is due to the differences in the discrete structure at the Gd/Fe interface and for the Fe atoms at the outer surface. This similarity of results remains appropriate for larger structures as well where one finds canted states for both lattice types. We conclude that although the quantitative values do change somewhat with lattice type, all the important qualitative features are present in both lattices. In calculations compared to experimental results, one generally has to introduce some tunable parameters that take this and other features into account. For example, the magnetic properties for both Fe and Gd in thin films and at interfaces are often different from their bulk values [26–28] and vary with the manufacturing technique.

(2) In our calculations we have neglected magnetocrystalline anisotropy. For single crystals, both Gd and Fe display a fairly small bulk anisotropy [29,30], below about 300 Oe, and the interface anisotropy has been estimated to be zero [26]. In previous calculations good agreement with experimental results has been found for polycrystalline thin films of Fe using a magnetocrystalline anisotropy ranging from 0 to 50 Oe [31] and neglecting any anisotropy in Gd. All of these values are generally small compared to the exchange and applied fields used in this paper.

(3) We have used a value of $J_i/k_B = -100$ K instead of the $J_i/k_B = -200$ K as in Ref. [9]. Figure 7(b) shows calculations comparing these two values of the interface exchange and very similar behavior is seen. Here the Fe core has a radius of 27 atoms, the Gd shell has a thickness of 4 atoms, and there is a 2 kOe applied field.

(4) We have assumed that the dipolar interactions are negligible in our structures. We have performed a calculation including dipolar interactions for a small structure, where a canted state is present. We chose this structure because we presumed that a canted state would be the most sensitive to dipolar fields while still being a small structure which is not too computationally demanding. This is compared to a similar calculation neglecting dipolar interactions, shown in Fig. 7(c). We again see the results are nearly identical. For this calculation the Gd core has a radius of 11 atoms, the Fe shell has a thickness of 4 atoms, and a 5 kOe applied field is present.

IV. CONCLUSION

We have used self-consistent local mean-field theory to model bimagnetic nanoparticles with AFM coupling at the interface. For spherical geometries we see that there are both surface effects and interface effects and multiple stable states. We have shown a core-shell particle which transitions between Fe-aligned, Gd-aligned, and canted states using a representative line of spins through the center of the particle. In addition, we have found that the compensation temperature of the particle can be varied over greater than a 300 K range by combinations of changing the volume ratio of the core and shell materials and by changing the applied field. The slope of the m vs T curves can also be made to increase, decrease, or remain approximately constant over a range of several hundred kelvins with this technique.

To contrast the interface-specific effects due to the AFM coupling between these two materials we compared a core-shell nanoparticle with an alloyed particle of the same size and volume fraction of material. We found that particles in a core-shell configuration can have a larger high-temperature magnetic moment than alloyed particles. For most alloyed particles there is no compensation temperature while a much richer behavior is seen in the bimagnetic particles.

The presence of a compensation temperature that can be tailored to specific temperatures suggests this type of nanoparticle could be used in a variety of applications. One such application would be as a contrast agent for MRI where the temperature range of interest is near the compensation temperature of nanoparticles. The nanoparticle creates a tunable dipole field, by varying the temperature or applied magnetic field, that acts on the nearby spins, changing the MRI signal. Analysis of the MRI signal will then yield information about local environment such as temperature measurements.

We also investigated the thermal stability of the nanoparticles and find that even at low applied fields (2 kOe) and with ideal nanoparticles with a radius of 7 atoms there is an appreciable magnetic moment which persists above the compensation temperature for Fe-Gd core-shell nanoparticles. We find that as the size of the nanoparticle is decreased the applied field necessary to induce a canted state increases.

[1] V. Markovich, R. Puzniak, D. Mogilyansky, X. Wu, K. Suzuki, I. Fita, A. Wisniewski, S. Chen, and G. Gorodetsky, J. Phys. Chem. C **115**, 1582 (2011).

[2] T. Kampfrath, M. Battiato, P. Maldonado, G. Eilers, J. Notzold, S. Mahrlein, V. Zbarsky, F. Freimuth, Y. Mokrousov, S. Blugel, M. Wolf, I. Radu, P. M. Oppeneer, and M. Munzenberg, Nat. Nanotechnol. **8**, 256 (2013).

[3] Q. Song and Z. J. Zhang, J. Am. Chem. Soc. **134**, 10182 (2012).

[4] E. Lima, E. L. Winkler, D. Tobia, H. E. Troiani, R. D. Zysler, Elisabetta Agostinelli, and Dino Fiorani, Chem. Mater. **24**, 512 (2012).

[5] M. Charilaou and F. Hellman, Phys. Rev. B **87**, 184433 (2013).

[6] Q. A. Pankhurst, J. Connolly, S. K. Jones, and J. Dobson, J. Phys. D: Appl. Phys. **36**, R167 (2003).

[7] K. M. Krishnan, IEEE Trans. Magn. **46**, 2523 (2010).

[8] J. H. Hankiewicz, Z. Celinski, K. F. Stupic, N. R. Anderson, and R. E. Camley, Nat. Commun. **7**, 12415 (2016).

[9] M. Sajieddine, Ph. Bauer, K. Cherifi, C. Dufour, G. Marchal, and R. E. Camley, Phys. Rev. B **49**, 8815 (1994).

[10] Y. Hu and A. Du, J. Appl. Phys. **110**, 033908 (2011).

[11] R. E. Camley and D. R. Tilley, Phys. Rev. B **37**, 3413 (1988).

[12] K. L. Krycka, R. A. Booth, C. R. Hogg, Y. Ijiri, J. A. Borchers, W. C. Chen, S. M. Watson, M. Laver, T. R. Gentile, L. R. Dedon, S. Harris, J. J. Rhyne, and S. A. Majetich, Phys. Rev. Lett. **104**, 207203 (2010).

[13] M. Estrader, A. López-Ortega, S. Estradé, I. V. Golosovsky, G. Salazar-Alvarez, M. Vasilakaki, K. N. Trohidou, M. Varela, D. C. Stanley, M. Sinko, M. J. Pechan, D. J. Keavney, F. Peiró,

S. Suriñach, M. D. Baró, and J. Nogués, Nat. Commun. **4**, 3960 (2013).
[14] O. Akdogan, A. Dobrynin, D. Le Roy, N. M. Dempsey, and D. Givord, J. Appl. Phys. **115**, 17A764 (2014).
[15] Y. Hu, G. Z. Wu, Y. Liu, and A. Du, J. Appl. Phys. **111**, 053904 (2012).
[16] H. M. Nguyen, C. H. Lee, P. Y. Hsiao, and M. H. Phan, J. Appl. Phys. **110**, 043909 (2011).
[17] M. Vasilakaki and K. N. Trohidou, Phys. Rev. B **79**, 144402 (2009).
[18] G. Binasch, P. Grünberg, F. Saurenbach, and W. Zinn, Phys. Rev. B **39**, 4828 (1989).
[19] A. Zaim, M. Kerouad, and Y. El Amraoui, J. Magn. Magn. Mater. **321**, 1077 (2009).
[20] F. C. Medeiros Filho, L. L. Oliveira, S. S. Pedrosa, G. O. G. Rebouças, A. S. Carriço, and A. L. Dantas, Phys. Rev. B **92**, 064422 (2015).
[21] D. C. Higgs, S. Bonetti, H. Ohldag, N. Banerjee, X. L. Wang, A. J. Rosenberg, Z. Cai, J. H. Zhao, K. A. Moler, and J. W. A. Robinson, Sci. Rep. **6**, 30092 (2016).
[22] C. Kittel, *Introduction to Solid State Physics* (Wiley, Hoboken, NJ, 2004).
[23] H. R. Kirchmayr and C. A. Poldy, J. Magn. Magn. Mater. **8**, 1 (1978).
[24] T. Ke-Qin, Z. Ke-Hua, C. Yan-Ming, and H. Zhi-Gao, Chin. Phys. B **23**, 056301 (2014).
[25] A. H. Morrish, *The Physical Principles of Magnetism*, Vol. 1 (John Wiley and Sons, Piscataway, NJ, 1965).
[26] S. Honda, M. Nawate, and I. Sakamoto, J. Appl. Phys. **79**, 365 (1996).
[27] A. Aspelmeier, F. Gerhardter, and K. Baberschke, J. Magn. Magn. Mater. **132**, 22 (1994).
[28] H. E. Nigh, S. Legvold, and F. H. Spedding, Phys. Rev. **132**, 1092 (1963).
[29] J. J. M. Franse and R. Gersdorf, Phys. Rev. Lett. **45**, 50 (1980).
[30] J. Ye, A. J. Newell, and R. T. Merrill, Geophys. Res. Lett. **21**, 25 (1994).
[31] R. E. Camley, W. Lohstroh, G. P. Felcher, N. Hosoito, and H. Hashizume, J. Magn. Magn. Mater. **286**, 65 (2005).